Oral Oncology 50 (2014) 848–856

Contents lists available at ScienceDirect

Oral Oncology

journal homepage: www.elsevier.com/locate/oraloncology

Assessment of the sensitivity and specificity of tissue-specific-based and anatomical-based optical biomarkers for rapid detection of human head and neck squamous cell carcinoma

Fangyao Hu [a,1], Karthik Vishwanath [a,1], H. Wolfgang Beumer [b], Liana Puscas [b,c], Hamid R. Afshari [d], Ramon M. Esclamado [b], Richard Scher [b], Samuel Fisher [b], Justin Lo [a], Christine Mulvey [a], Nirmala Ramanujam [a], Walter T. Lee [b,c,*]

[a] Duke University, Biomedical Engineering Department, Durham, NC, USA
[b] Division of Otolaryngology – Head and Neck Surgery, Duke University Medical Center, Durham, NC, USA
[c] Section of Otolaryngology – Head and Neck Surgery, Durham Veterans Administration Medical Center, Durham, NC, USA
[d] Dental Service, Durham Veterans Administration Medical Center, Durham, NC, USA

ARTICLE INFO

Article history:
Received 31 October 2013
Received in revised form 22 May 2014
Accepted 19 June 2014
Available online 16 July 2014

Keywords:
Diffuse reflectance
Head and neck cancer
Cancer detection
Hypoxia
Global health
Cancer screening

SUMMARY

Objectives: We propose the use of morphological optical biomarkers for rapid detection of human head and neck squamous cell carcinoma (HNSCC) by leveraging the underlying tissue characteristics in aero-digestive tracts.

Materials and Methods: Diffuse reflectance spectra were obtained from malignant and contra-lateral normal tissues of 57 patients undergoing panendoscopy and biopsy. Oxygen saturation, total hemoglobin concentration, and the reduced scattering coefficient were extracted. Differences in malignant and normal tissues were examined based on two different groupings: anatomical site and morphological tissue type.

Results and Conclusions: Measurements were acquired from 252 sites, of which 51 were pathologically classified as SCC. Optical biomarkers exhibited statistical differences between malignant and normal samples. Contrast was enhanced when parsing tissues by morphological classification rather than anatomical subtype for unpaired comparisons. Corresponding linear discriminant models using multiple optical biomarkers showed improved predictive ability when accounting for morphological classification, particularly in node-positive lesions. The false-positive rate was retrospectively found to decrease by 34.2% in morphologically- vs. anatomically-derived predictive models. In glottic tissue, the surgeon exhibited a false-positive rate of 45.7% while the device showed a lower false-positive rate of 12.4%. Additionally, comparisons of optical parameters were made to further understand the physiology of tumor staging and potential causes of high surgeon false-positive rates. Optical spectroscopy is a user-friendly, non-invasive tool capable of providing quantitative information to discriminate malignant from normal head and neck tissues. Predictive models demonstrated promising results for real-time diagnostics. Furthermore, the strategy described appears to be well suited to reduce the clinical false-positive rate.

Published by Elsevier Ltd.

Introduction

In 2012, there were 52,610 new cases of mucosal head and neck cancers (HNC) in the United States [1]. These cancers develop through a spectrum of changes that can be pathologically identified as progressing from hyperplasia to dysplasia to carcinoma *in situ*, and finally, to invasive carcinoma [2–4]. Once carcinoma is identified, treatment currently involves modalities of surgery, radiation, and chemotherapy [3]. Early detection of new and locally recurrent cancers is clinically important to reduce not only cancer related mortality, but also treatment associated morbidity, as it impacts multiple organ functions including respiration, olfaction, hearing, eating, swallowing, and speaking [5].

The gold standard for diagnosing cancer is dependent on pathological examination. Thus, currently all patients with clinically suspicious lesions undergo surgical biopsies. Although these

* Corresponding author at: Division of Otolaryngology – Head and Neck Surgery, Duke University Medical Center, Duke Clinics Blue Zone – 3561b, Durham, NC 27710, USA. Tel.: +1 919 681 8449 (O); fax: +1 919 681 7949.
E-mail address: walter.lee@duke.edu (W.T. Lee).
[1] Contributed equally to this research.

http://dx.doi.org/10.1016/j.oraloncology.2014.06.015
1368-8375/Published by Elsevier Ltd.

lesions are identified during an initial clinical exam, obtaining a specimen via biopsy for analysis can be uncomfortable for patients. This may further include the use of labor, facility, and monetary resources that are expended on patients, some of whom may ultimately have no malignancy. It would be of benefit to clinicians and patients if it were possible to have an "adjunct" technique that could suitably identify those patients that would benefit from further surgical biopsy from those that likely only need follow-up clinical observations. For those patients identified as having a low likelihood of cancer, this would prevent unnecessary procedures, pain, and better utilize limited resources. The clinical value of this tool would depend on it providing rapid, non-invasive feedback could be obtained during the patient's visit. This would be facilitated by a portable unit such that it can be used in ambulatory settings, and quantitative such that data obtained is consistent across operators and patients.

Several techniques show potential in non-invasive cancer diagnoses. Fluorescence endoscopy relies on contrast agents for staining and imaging cell nuclei [6,7]. Time-domain Optical coherence tomography (OCT) system requires a Michelson interferometer to sample lesions in z-direction [8]. Frequency-domain OCT system improve the image acquisition time, where information in the z-direction is sampled in the spatial frequency domain [9]. Reflectance confocal microscopy utilizes a pinhole to reject the out-of-focus light [10,11]. Hence, the cellular structures could be imaged in nontransparent tissues. Although these techniques show high potential in cancer diagnoses [6,12,13], the systems is expensive or requiring extra procedures. Moreover, these techniques provide only the morphological information but not the physiological information.

Diffuse reflectance spectroscopy (DRS) can provide information about tissue composition including physiological, metabolic and structural properties [14]. DRS has been used to show that malignant and normal tissues of the head and neck can be differentiated when analyzed using a variety of different techniques [15–32]. Our team has developed a quantitative DRS technique that incorporates a portable fiber-based spectrometer and a robust inverse Monte Carlo (MC) algorithm capable of extracting tissue optical properties [33,34]. The inverse model can rapidly compute total hemoglobin concentration (THb), hemoglobin oxygen saturation (SO_2), and mean reduced tissue scattering coefficient (μ_s'), which reflects the cellularity of the tissue within the probed volume. The feasibility of using DRS in patients undergoing panendoscopy has been demonstrated [16].

Although the majority of HNC are squamous cell carcinomas (>90%), signals collected from DRS might be sensitive to both SCC and the underlying tissues (the tissue below the epithelial cancer) since DRS usually lacks of optical sectioning ability. Current description of head and neck squamous cell carcinomas (HNSCC) is often based on anatomical boundaries (i.e. oropharynx, oral cavity, pharynx, larynx) [35]. Therefore, contrast detected by DRS between the tumor and normal tissues might be diminished when mixing samples with different surrounding tissue types. Other groups have tried to eliminate the effects of collecting light from beneath the epithelium when trying to diagnose epithelial cancers. Perelman et al. employed a physical model for the diffusive background originated from the stroma [36]. After removing the background, density and size distribution of the nuclei can be computed, though this method is time-consuming. Nieman et al. combined an angled illumination-collection strategy with the polarization illumination technique for reducing the optical background signals from the stromal layer [37]. Nevertheless, an angled illumination-collection probe with polarization sensitivity technique is hard to fabricate. We simply propose that by grouping the samples with similar tissue types, contrast between the SCC and normal tissues could be enhanced.

In this manuscript, the diagnostic accuracy between the anatomical and tissue-specific grouping strategies using the optical biomarkers obtained via the quantitative DRS technique was investigated for the HNSCC detection during staging panendoscopy. In addition, a comparison was made among the optical biomarkers of normal, node-positive, and node-negative malignant tissues. Finally, optical biomarkers of the malignant, pathologically confirmed normal, and clinically observed normal tissue samples were compared.

Materials and methods

Clinical study design

This study was approved by the Duke University School of Medicine Institutional Review Board (Pro00021026) and was open to all patients who were scheduled for panendoscopy and biopsy for suspected HNC at the Duke University Hospital during 2010–2012. Patients with suspicious lesions were approached and consented to undergo a non-invasive evaluation of sites to be biopsied using the optical probe. All patients were included in the study with no further sub-selection. Tissue biopsies were only obtained from the site suspected of disease and all measurements from normal appearing unaffected tissues were assumed to be normal. No biopsies were taken from normal appearing unaffected tissues. Several surgeons specialized in head and neck surgery participated in this study taking biopsies. The locations of distant normal tissue measurements were supervised by the same surgeon (W.L.) who participated in a previously published study at the Durham Veterans Administration Hospital [16] in which 25 normal tissues were biopsied and submitted for histopathology. In this study, the surgeon demonstrated 100% accuracy in correctly identifying clinically-appearing distant normal sites as histologically normal.

In each consented patient, the optical probe was placed on the surface of at least two tissue sites ("tumor" and "normal appearing unaffected tissue"). Five diffuse reflectance scans were obtained at each site and data was recorded. To co-localize the optical scans and clinical biopsies, the suspicious sites were biopsied immediately after the optical measurements were completed with the attending physician visually marking the spot of optical measurements for biopsy (which was approximately 2–5 mm in diameter).

The measurements were obtained from anatomical sites in the larynx, pharynx, or oral cavity. Four groups were built based on the structures underneath the epithelium layer and their epithelial variations. The first group consisted of measurements from the glottis. Specialized structures existed such as vocal cord in the larynx area. The true and false vocal cords are covered with stratified squamous epithelium and the ciliated pseudostratified columnar epithelium respectively [38]. The supporting ligament and muscle, vocalis muscle, also makes the underlying of the vocal cord different from the other structures in head and neck. The second lymphoid group was formed by combining measurements from the oropharynx, tonsil and base of the tongue due to the rich lymphatic drainage in the region [39]. The third muscle group consisted of measurements from tongues which consisted of majorly with striated muscle fibers. The tongue epithelium, which is modified into filiform papillae and fungiform papilla, is also distinct from other epitheliums in head and neck. The last group combined measurements from all remaining sites into a mucosal group.

Optical spectroscopy instrumentation

A portable fiber optic instrument (Fig. 1) was used to measure tissue diffuse reflectance spectra. Light from a 40 W halogen lamp (HL2000HP; Ocean Optics, Dunedin, FL), was coupled to an optical

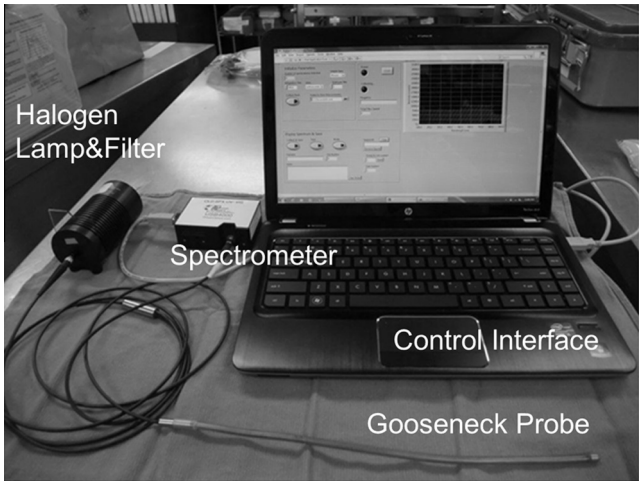

Figure 1. A picture of the portable system which consists of a laptop, USB spectrometer, halogen light source, heat filter and a bendable gooseneck probe containing the two optical fibers. The system is computer controlled.

fiber (400 μm diameter) for illumination. Another fiber (400 μm diameter) was placed 475 μm away from the source fiber and coupled the diffuse reflectance from tissue into a spectrometer (USB4000, Ocean Optics, Dunedin, FL). Tissue reflectance measurements were normalized to a 99% reflectance standard measurement (Labsphere, Inc.) obtained each day. Tissue sensing depths were determined using forward MC simulation [40] and were found to be 1.1 mm and 1.6 mm at 480 nm and 600 nm, respectively, for the median absorption and scattering coefficients derived from the previous study [16].

Extraction of tissue biomarkers from optical reflectance data

Diffuse reflectance spectra (480–650 nm) were collected and analyzed using an inverse MC model to obtain the scattering and absorption coefficients [33]. THb (μM), SO_2 (%) and μ_s' (1/cm) were extracted from the absorption and scattering coefficients [16].

Statistical analysis

Tissue samples were divided into malignant and normal groups, based on histopathological diagnosis of biopsied tissues and clinical impression of the non-biopsied normal tissues. The histopathological slides were read and analyzed by several pathologists from Duke Universality Medical Center Pathological laboratory. The pathologists and surgeons were blinded to the DRS results. Mean contributions per tissue/site for all extracted optical biomarkers were compared between groups using the Wilcox rank-sum test to determine if there were statistically significant differences ($p < 0.05$) between the two groups. Linear-discriminant models were used to classify the tissue as malignant or normal, by using all or a subset of (all pair-wise combinations of THb, SO_2, and μ_s') the three optical biomarkers. This was carried out for tissues grouped by the anatomical sites classification (larynx, pharynx, oral) and for tissues grouped by the tissue-specific classification (lymphoid, glottis, mucosal and muscle). The sensitivity (Se), specificity (Sp), positive predict value (PPV) and negative predict value (NPV) were determined by comparing the model prediction to the pathological diagnosis. The discriminant algorithm was validated using a leave-one-out cross-validation technique. In addition, the optical biomarkers of the normal, the lymph-node-positive, and the lymph-node-negative samples were compared with the Wilcox rank-sum test. Finally, differences between the optical biomarkers of the normal, pathologically-confirmed normal and the clinical observed normal samples were also evaluated with the Wilcox rank-sum test. All data processing and statistical data analysis was performed using MATLAB (MathWorks Inc., Natick MA).

Results

Ninety-nine biopsies co-localized with optical probe measurements were obtained from the 57 enrolled patients. Fifty-one of the 99 biopsies were diagnosed as SCC. These 51 SCC samples were obtained from 37 of the enrolled patients. Forty of the 99 biopsies were pathologically classified as negative for SCC (30 pathologically-confirmed normal tissue, 10 inflammation with no atypia). No specific information regarding other pathology such as lichen planus, ulceration were specifically given in the pathology report. Eight of the 99 biopsies were pathologically classified as dysplastic, and these were excluded from this study due to the small sample size. Another 158 optical probe measurements were measured at distant normal epithelium from all 57 patients. These 158 sites were not biopsied and were considered to be normal based on clinical appearance and distance from the tumor.

Fig. 2 shows the representative normalized reflectance scans of malignant and nonmalignant tissues for the 3 anatomical sites and the 4 morphological categories. All SCC-positive tissues were further separated into 4 groups by their tumor size and lymph node status according to the TMN staging information. A breakdown by anatomical site, morphological categories, tumor stage and lymph node status for all measurements in this study is shown in Table 1.

Contrast between SCC and normal samples is significantly enhanced when grouped by tissue morphology

Fig. 3 shows SO_2, THb and μ_s' as boxplots when the samples were grouped together by anatomical sites or by morphologically-similar sites for pathologically-confirmed SCC and normal sites. When the samples were grouped by their anatomical locations, the SO_2 of the malignant tissues was significantly lower than that in normal tissues in the larynx and the pharynx ($p < 0.01$ for both). The μ_s' of the malignant tissues was significantly lower than that in the normal tissues in the pharynx ($p = 0.03$) and in the oral cavity ($p < 0.01$). When the samples were grouped by morphologically-similar tissue types, SO_2 showed statistically significant differences between SCC and normal tissues for all four tissue groups (glottis $p < 0.01$; lymphoid $p < 0.01$; muscle $p = 0.03$; and mucosal $p < 0.01$). Further, statistical differences in μ_s' were also observed between SCC and normal tissues of lymphoid and mucosal origin ($p = 0.02$ and $p < 0.01$, respectively) but not in the glottis. The μ_s' of the SCC tissues is nearly significantly lower than the μ_s' of the normal tissues ($p = 0.058$) in the muscle group. In summary, contrast between SCC and normal tissue is significantly enhanced when parsing tissues by morphological rather than by anatomical subtypes.

Linear discriminant model has better predictive power with the morphological tissue grouping

The sensitivity, specificity, PPV and NPV were computed by comparing predictions from the discriminant model to those obtained from pathology and are listed for each set of optical variables used (Table 2). The numbers of false negative (FN) and false positive (FP) samples are also provided. The FNs were separated into node-positive SCC and node-negative SCC for Tis/T1/T2 stage and T3/T4 stage. The FPs were separated into pathologically nor-

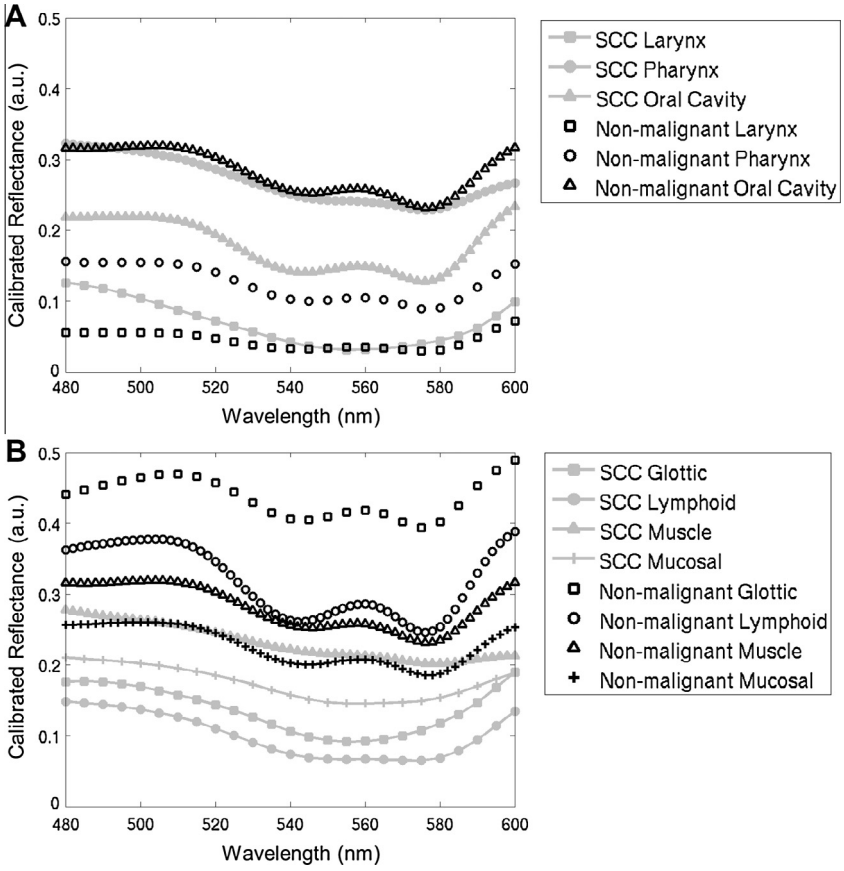

Figure 2. Representative normalized reflectance scans for the 3 anatomical sites (A) and the 4 morphological categories (B).

Table 1
Breakdown of anatomical site, sub-site and morphologically similar tissue types for all measurements. All tumor sites were confirmed by histopathological confirmation of biopsies. 37 patients had pathologically-confirmed SCC. The number of patients included in each sample type was indicated in the parentheses.

			Pathology confirmed SCC					Normal		
			Tis/T1/T2[a]		T3/T4		Total	Pathology confirmed	Clinical observation	Total
Anatomical site	Anatomical sub-site	Morphological groups	N+[b]	N−[c]	N+	N−				
Larynx	Glottic	Glottic	1(1)	11(8)	2(1)	0(0)	14(10)	21(14)	23(18)	47(23)
	Supraglottic	Mucosal	2(2)	1(1)	2(2)	0(0)	5(5)	0(0)	5(4)	5(4)
	Site-total		3(2)	12(8)	4(3)	0(0)	19(13)	21(14)	28(21)	52(25)
Pharynx	Oropharynx	Lymphoid	2(2)	0(0)	1(1)	0(0)	3(3)	1(1)	7(6)	8(6)
	Hypopharynx	Mucosal	1(1)	0(0)	0(0)	0(0)	1(1)	3(2)	1(1)	4(3)
	Base of Tongue	Lymphoid	5(5)	3(3)	2(2)	0(0)	10(10)	11(7)	15(14)	26(15)
	Tonsil	Lymphoid	3(3)	1(1)	1(1)	1(1)	6(6)	0(0)	5(4)	5(4)
	Site-total		11(11)	4(4)	4(3)	1(1)	20(19)	15(8)	28(22)	43(23)
Oral cavity	Tongue	Muscle	3(1)	4(3)	0(0)	0(0)	7(4)	3(2)	34(29)	37(29)
	Floor of Mouth	Mucosal	0(0)	0(0)	1(1)	0(0)	1(1)	0(0)	23(22)	23(22)
	Alveolus	Mucosal	0(0)	0(0)	0(0)	2(1)	2(1)	0(0)	2(2)	2(2)
	Palate	Mucosal	0(0)	0(0)	0(0)	0(0)	0(0)	1(1)	21(19)	22(19)
	Cheek	Mucosal	0(0)	1(1)	0(0)	0(0)	1(1)	0(0)	22(22)	22(22)
	RMT[d]	Mucosal	0(0)	1(1)	0(0)	0(0)	1(1)	0(0)	0(0)	0(0)
	Site-total		3(1)	6(5)	1(1)	2(1)	12(8)	4(3)	102(34)	106(34)
Total			17(14)	22(17)	9(6)	3(2)	51(37)	40(25)	158(56)	198(57)

[a] Tis: carcinoma *in situ*.
[b] N+: node-positive SCC.
[c] N−: node-negative SCC.
[d] RMT: retromolar trigone.

mal and clinically normal groups. Overall, for every pair of optical variables selected, there were improvements in the sensitivity, specificity, PPV, and NPV when discriminant models were built based on morphological groupings, relative to a model that was built based on the anatomical location. The total number of FN samples was lowest when using all three optical biomarkers for classification. Importantly, the total number of FNs and FPs derived from the morphologically-grouped algorithm was less than the total number of FNs and FPs derived from anatomically-grouped algorithm. Further, the algorithm based on morphological groupings was particularly more effective in identifying node-positive vs. node-negative disease.

Table 2
Diagnostic accuracy based on linear-discriminant models using two or more measured optical biomarkers for sites grouped by anatomical sites or by tissue types (shaded cells). The sensitivity, specificity, positive predictive value and negative predictive value values are reported for leave-one-out cross-validation. The standard error of the diagnostic accuracies were computed and provided in the parentheses. The numbers in the site column in parenthesis represents the number of node positive SCC, node-negative SCC, pathologically-confirmed normal, clinically-observed normal samples in each group. See Table 1 for tissue groupings used. The numbers of false negatives and false positives are also shown. The FN was further broken down into N+ and N− groups. The FP was broken down into pathological confirmed normal or clinical observed normal groups. The collective Se, Sp, PPVs and NPVs when all subgroups are combined are also shown. This table suggests that while the same optical biomarkers were used to build the discriminant model, the models generally perform better when the samples were grouped by tissue type (shaded) than by anatomical site (non-shaded). Moreover, the discriminant models with three optical biomarkers generally classify the samples better than those with only two optical biomarkers. The number in parenthesis indicates the standard error of the corresponding diagnostic accuracy.

						FN					FP		
						Tis/T1/T2		T3/T4		Total	[a]Path.	[b]Clin.	Total
Biomarker Pairs	Site	Se.	Sp.	PPV.	NPV.	N+	N-	N+	N-				
SO_2&THb	Larynx (7/12/24/28)	63%(11.1%)	94%(3.4%)	80%(10.3%)	88%(4.7%)	1	4	2	0	7	2	1	3
	Pharynx (15/5/15/28)	65%(10.6%)	86%(5.3%)	68%(10.7%)	84%(5.5%)	4	1	1	1	7	4	2	6
	Oral Cavity (4/8/4/102)	50%(14.4%)	73%(4.3%)	17%(6.4%)	93%(2.8%)	1	4	0	1	6	1	28	29
	Total	61%(6.8%)	81%(2.8%)	45%(6.0%)	89%(2.3%)	6	9	3	2	20	7	31	38
	Glottic (3/11/24/23)	57%(13.2%)	94%(3.8%)	73%(13.4%)	88%(4.7%)	1	4	1	0	6	2	1	3
	Lymphoid (14/5/12/27)	68%(10.6%)	87%(5.4%)	72%(10.6%)	85%(5.6%)	3	1	1	1	6	3	2	5
	Muscle (3/4/3/34)	71%(17.1%)	68%(7.7%)	29%(11.1%)	93%(5.0%)	1	1	0	0	2	0	12	12
	Mucosal (6/5/4/74)	73%(13.4%)	90%(3.4%)	50%(12.5%)	96%(2.3%)	0	2	0	1	3	2	6	8
	Total	67%(6.6%)	86%(2.5%)	55%(6.3%)	91%(2.1%)	5	8	2	2	17	7	21	28
SO_2&μ_s'	Larynx (7/12/24/28)	63%(11.1%)	94%(3.4%)	80%(10.3%)	88%(4.7%)	1	4	2	0	7	2	1	3
	Pharynx (15/5/15/28)	75%(9.7%)	86%(5.4%)	71%(9.9%)	88%(5.0%)	2	1	1	1	5	5	1	6
	Oral Cavity (4/8/4/102)	67%(13.6%)	74%(4.3%)	22%(6.9%)	95%(2.4%)	1	2	0	1	4	2	26	28
	Total	69%(6.5%)	82%(2.8%)	49%(5.9%)	91%(2.2%)	4	7	3	2	16	9	28	37
	Glottic (3/11/24/23)	57%(13.2%)	94%(3.8%)	73%(13.4%)	88%(4.9%)	1	4	1	0	6	2	1	3
	Lymphoid (14/5/12/27)	74%(10.1%)	87%(5.4%)	74%(10.1%)	87%(5.4%)	2	1	1	1	5	4	1	5
	Muscle (3/4/3/34)	71%(17.1%)	73%(7.3%)	33%(12.1%)	93%(4.7%)	1	1	0	0	2	0	10	10
	Mucosal (6/5/4/74)	73%(13.4%)	92%(3.0%)	57%(13.2%)	96%(2.3%)	0	2	0	1	3	3	3	6
	Total	69%(6.5%)	88%(2.6%)	59%(6.5%)	92%(2.0%)	4	8	2	2	16	9	15	24
SO_2&THb&μ_s'	Larynx (7/12/24/28)	63%(11.6%)	94%(3.4%)	80%(10.3%)	88%(4.7%)	1	4	2	0	7	2	1	3
	Pharynx (15/5/15/28)	80%(8.9%)	86%(5.3%)	73%(9.5%)	90%(4.6%)	1	1	1	1	4	5	1	6
	Oral Cavity (4/8/4/102)	67%(13.6%)	73%(4.3%)	22%(6.8%)	95%(2.4%)	1	2	0	1	4	2	27	29
	Total	71%(6.4%)	81%(2.8%)	49%(5.8%)	92%(2.1%)	3	7	3	2	15	9	29	38
	Glottic (3/11/24/23)	57%(13.2%)	94%(3.8%)	73%(13.4%)	88%(4.9%)	1	4	1	0	6	2	1	3
	Lymphoid (14/5/12/27)	79%(9.4%)	90%(4.9%)	79%(9.4%)	90%(4.9%)	1	1	1	1	4	3	1	4
	Muscle (3/4/3/34)	71%(17.1%)	73%(7.3%)	33%(12.2%)	93%(4.7%)	1	1	0	0	2	0	10	10
	Mucosal (6/5/4/74)	73%(13.4%)	90%(3.4%)	50%(12.5%)	96%(2.3%)	0	2	0	1	3	3	5	8
	Total	71%(6.4%)	88%(2.4%)	59%(6.3%)	92%(2.0%)	3	8	2	2	15	8	17	25

[a] Path.: pathological confirmed normal sample.
[b] Clin.: clinical observed normal samples.

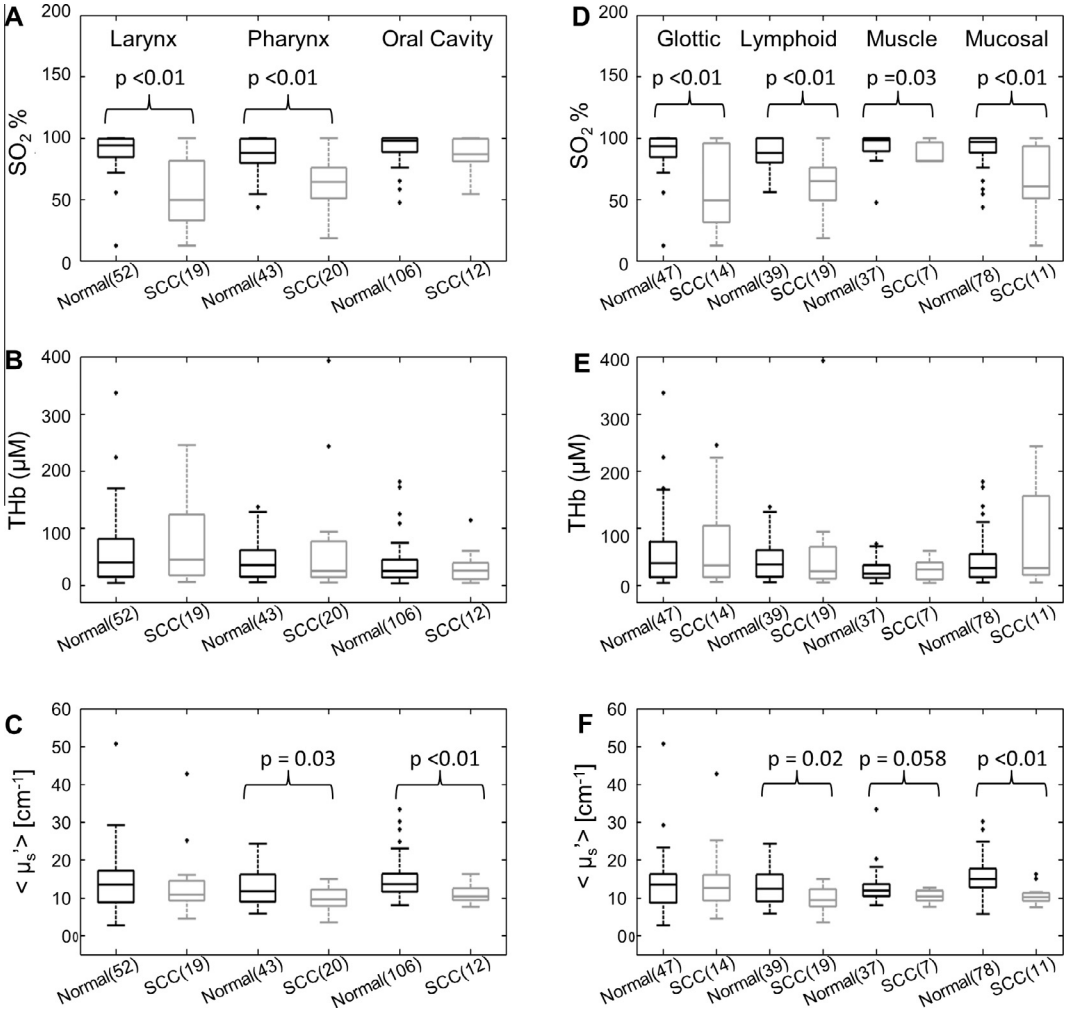

Figure 3. Range and median values of extracted biomarkers for normal and SCC for different anatomic and tissue classifications. Numbers in parentheses indicate sample numbers. Significant *p*-values are reported from unpaired Wilcoxon rank sum tests. Contrast between SCC and normal tissues is enhanced when parsing tissues by morphological rather than by anatomical subtypes ($^{*}p < 0.05$, $^{**}p < 0.01$) (N: normal).

Tissue scattering and hemoglobin oxygenation saturation are lower at the primary tumor with node positive disease

Fig. 4 shows boxplots of the optical biomarkers for normal samples, node-positive and node-negative SCC samples. The SO_2 of the normal samples was significantly higher than that of the node-positive and node-negative SCC groups ($p < 0.01$ for both). The μ_s' of the node-positive SCC samples was nearly significantly lower than that of normal group ($p = 0.055$) thus providing additional contrast when differentiating normal from node-positive SCC samples. Moreover, the μ_s' of the node-positive SCC samples was significantly lower than that of node-negative SCC samples ($p < 0.01$) and the μ_s' of the node-negative SCC samples was significantly lower than that of the normal samples ($p < 0.01$).

Optical spectroscopy shows contrast between SCC and pathologically-confirmed normal tissues

Fig. 5 shows boxplots of the optical parameters for the malignant, pathologically-confirmed normal and clinically-observed normal tissues. The SO_2 of the malignant tissues were significantly lower than both the pathological normal tissues and the clinical observed normal tissues. The SO_2 of the pathological normal tissues were also significantly lower than the clinically-observed normal tissues. No statistical significance was observed in the THb results. The μ_s' of the clinically-observed normal tissues were higher than both the pathologically-confirmed normal and the malignant tissues.

Discussion

Our results show that when using SO_2, THb and μ_s' for building the discriminant models, the overall PPV and NPV increased from 49% and 92%, respectively, to 59% and 92%, when tissue-specific classification was used instead of anatomically-based classification. Moreover, this change resulted in a 34% decrease in the number of FP classifications. This supports the hypothesis that a strong predictive algorithm would need to be tissue-specific, since different tissues are expected to have different baseline physiological and morphological properties. It has been demonstrated that these differences in morphological and chemical properties affects the tissue optical properties. For instance, Bashkatov et al. showed that the absorption and the scattering spectra of human skin, subcutaneous adipose, and mucosa exhibit different spectral features [41]. Therefore, mixing different types of tissues could be expected to diminish contrast between the malignant and normal tissues as observed here.

Forty-three clinically-appearing malignant tissues were confirmed to be histologically benign. While the tissue absorption and scattering were similar between the 51 malignant and the

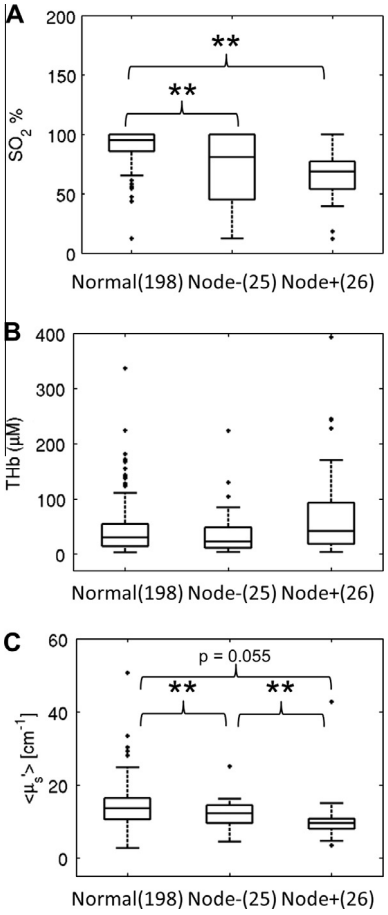

Figure 4. Boxplots of SO_2 (A), THb (B) and μ_s'(C) for normal and SCC samples. The SCC samples were separated into two groups by lymph node status. The significant p values from Wilcoxon rank sum tests are shown. This figure suggests that head and neck malignant tissue is generally hypoxic. Moreover, as the tumor progress from node-negative to node-positive, the tissue scattering generally decreases. ($^{**}p < 0.01$) (N: normal).

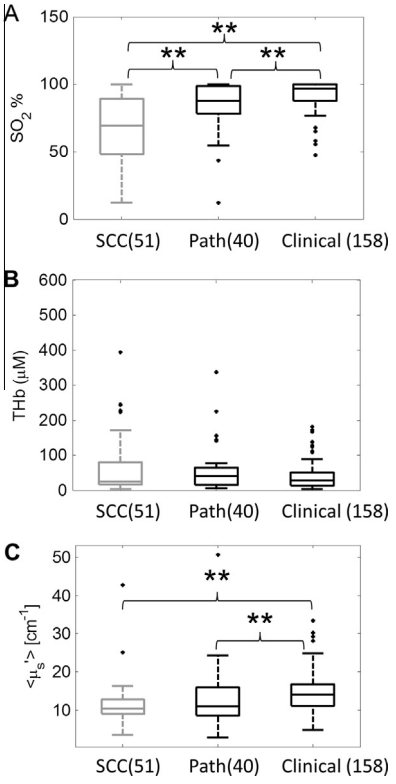

Figure 5. Boxplots of SO_2 (A), THb (B) and μ_s'(C) for malignant, pathologically-confirmed normal and clinically-observed normal tissue. The significant p values computed from the Wilcoxon rank sum tests are shown. ($^{**}p < 0.01$) This figure suggests that the contrast between the malignant and pathologically-confirmed normal was less than the contrast between the malignant and the clinically-observed normal tissues. (Path.: pathologically-confirmed normal. Clinical: clinical observed normal).

43 pathologically-confirmed normal tissues, the SO_2 was significantly different. The algorithm based on morphological groupings classified 81% of these samples correctly. In addition, 23 glottic samples were biopsied and confirmed as pathologically normal. With the morphologically based algorithm, only 2 pathologically-confirmed benign samples were classified as malignant. This implies that the vast majority of these glottic biopsies if obtained for the concern of cancer may have been avoided. These data illustrate the potential utility of using optical spectroscopy for reducing the number of biopsies and their related patient discomfort/pain and use of limited resources.

The effect of enhancing contrast when building the linear discriminant model based on tissue type is obvious when comparing the oral cavity group to its constituent tissue groups (muscle and mucosal) since they had comparable sample sizes (37% muscle, 63% mucosal). The linear discriminant models have better sensitivities and PPVs and similar specificities and NPVs regardless of the optical parameters chosen (Table 2) when using tissue type over anatomical location. In addition, the SO_2 showed no statistical differences between the malignant and normal tissues in the oral cavity. On the other hand, both the SO_2 of the malignant tissues in muscle and the mucosal group were significantly lower than the SO_2 of the normal tissues in the corresponding group (Fig. 3).

Optical techniques have been widely used to detect and characterize differences between dysplastic and malignant tissue from benign tissue, as reviewed previously [35,42,43]. Although capable of providing high discriminatory power, these approaches rely on heuristic algorithms for classification, and do not necessarily leverage information about the underlying tissue physiology or morphology for tissue classification, as has been demonstrated in this study. Further, only one of the three groups mentioned above has previously reported on differences between benign and dysplastic and/or cancerous lesions based on anatomical sub groups. However, this was limited to just the oral cavity, which is a very small subset of the head and neck lesions observed clinically.

Hypoxia is a general characteristic of solid tumors in the head and neck [44] due to a less-ordered and leaky vascular supply, as compared with that of normal tissues [45]. In this manuscript, the oxygenation of the malignant head and neck tissues are shown to be generally lower than that of normal head and neck tissues in the unpaired comparisons (Figs. 3–5). This result was also observed in our previous spectroscopy study of HNCC [16]. In another study, Terris and Dunphy found that the pO_2 of the primary tumor (22.7 ± 16.0 mm Hg) was lower than that of normal subcutaneous tissue (57.2 ± 12.8 mm Hg) [46]. This result is concordant with our findings. In addition to providing contrast for the detection of SCC, knowledge of tumor SO_2 will be invaluable in therapy planning, as tumor hypoxia renders the tumor resistant to radiation treatment, which plays an important role in HNC therapy.

Tissue scattering likely reflects the morphology of the HNC. Tissue scattering of the malignant tissues was significantly lower than that of the clinical observed normal tissues. Moreover, tissue scattering of lymph-node-positive malignant tissues was lower than both normal tissues and node-negative malignant tissues. This could be caused by the loss of collagen in the basement membrane during the invasion of the SCC cells. Breach of the basement

membrane is considered to be the first step for the HNSCC cells to become an invasive carcinoma [47,48]. Both urokinase-type plasminogen activator and metalloproteinases (MMPs, also known as collagenases) play important roles allowing SCC cells to degrade the basement membrane. Activating the urokinase or the collagenases can result in the hydrolysis of collagen [49,47,50], which serves as an important component in the basement membrane and one major tissue scatterer as well [51]. Georgakoudi et al. observed a decrease of tissue scattering during the progression of dysplasia in esophagus tissue with reflectance spectroscopy [52]. Loss of collagen due to neoplasia can also be seen in wide-field autofluorescence imaging in oral cavity [53].

Although we failed to achieve 100% sensitivity and specificity, our technique is low-cost, label-free and portable, and thus has potential in countries where histopathology services are limited. If our technique proves reliable and rapid screening, it could reduce the current burden of trained pathologists. In addition, the classification outcome may be improved by further refining the tissue grouping strategy. This strategy could also be applied to other technologies and organ sites. Moreover, our results show that the tissue scattering at the primary tumor might be related to the nodal status. This is important since whether the cancer has metastasized will significantly change the treatment strategy. Finally, current histopathology results of the biopsies at the primary tumor would not reveal the lymph node status.

Our group demonstrates a quantitative optical spectroscopy technique and tissue grouping strategy capable of enhancing contrast between malignant and normal tissues from different regions of the head and neck. In this preliminary diagnostic study, our data suggests that a predictive algorithm that combines optical endpoints and that is stratified by tissue type improves accuracy, particularly in node-positive disease. This is based on accounting for differences in tissue physiology and morphology within the upper aerodigestive tract. Further, the strategy described here appears to be particularly well suited to reduce the clinical false-positive rate, particularly for glottic tissue, where the surgeon had the highest false-positive rate, thereby potentially reducing the need for unnecessary surgical procedures that could significantly impact patient morbidity.

Role of the funding source

This work was funded by the Alexander and Margaret Stewart Trust, Duke Cancer Institute, and the NIH (5K99CA140783-02) (KV). This project was supported by Career Development Award (IK2BX001398) from the Biomedical Laboratory Research and Development Service of the Department of Veterans Affairs Office of Research and Development (WTL). The views expressed in this article are those of WTL and LP and do not necessarily represent the views of the Department of Veterans Affairs or the United States government.

Conflict of Interest

None declared.

References

[1] Cancer Facts and Figures. Atlanta, GA: American Cancer Society; 2008.
[2] Argiris A, Karamouzis MV, Raben D, et al. Head and neck cancer. Lancet 2008;371:1695–709.
[3] Forastiere A, Koch W, Trotti A, et al. Head and neck cancer. New Engl J Med 2001;345:1890–900.
[4] Hunter KD, Parkinson EK, Harrison PR. Profiling early head and neck cancer. Nat Rev Cancer 2005;5:127–35.
[5] Thompson LW. Head and neck cancer: early detection. Semin Surg Oncol 1989;5:168–75.
[6] Vila PM, Park CW, Pierce MC, et al. Discrimination of benign and neoplastic mucosa with a high-resolution microendoscope (HRME) in head and neck cancer. Ann Surg Oncol 2012;19:3534–9.
[7] Parikh ND, Perl D, Lee MH, et al. In vivo diagnostic accuracy of high-resolution microendoscopy in differentiating neoplastic from non-neoplastic colorectal polyps: a prospective study. Am J Gastroenterol 2014;109:68–75.
[8] Brezinski ME, Fujimoto JG. Optical coherence tomography: high-resolution imaging in nontransparent tissue. IEEE J Sel Top Quant 1999;5:1185–92.
[9] Yun SH, Tearney GJ, de Boer JF, et al. High-speed optical frequency-domain imaging. Opt Express 2003;11:2953–63.
[10] Clark AL, Gillenwater AM, Collier TG, et al. Confocal microscopy for real-time detection of oral cavity neoplasia. Clin Cancer Res 2003;9:4714–21.
[11] Rajadhyaksha M, Anderson RR, Webb RH. Video-rate confocal scanning laser microscope for imaging human tissues in vivo. Appl Opt 1999;38:2105–15.
[12] Ridgway JM, Armstrong WB, Guo S, et al. In vivo optical coherence tomography of the human oral cavity and oropharynx. Arch Otolaryngol 2006;132:1074–81.
[13] Gerger A, Koller S, Weger W, et al. Sensitivity and specificity of confocal laser-scanning microscopy for in vivo diagnosis of malignant skin tumors. Cancer 2006;107:193–200.
[14] Ramanujam N. Fluorescence spectroscopy of neoplastic and non-neoplastic tissues. Neoplasia 2000;2:89–117.
[15] Amelink A, Kaspers OP, Sterenborg HJCM, et al. Non-invasive measurement of the morphology and physiology of oral mucosa by use of optical spectroscopy. Oral Oncol 2008;44:65–71.
[16] Beumer HW, Vishwanath K, Puscas L, et al. Detection of squamous cell carcinoma and corresponding biomarkers using optical spectroscopy. Otolaryngol Head Neck 2011;144:390–4.
[17] Ghanate AD, Kothiwale S, Singh SP, et al. Comparative evaluation of spectroscopic models using different multivariate statistical tools in a multicancer scenario. J Biomed Opt 2011;16.
[18] Jayanthi JL, Nisha GU, Manju S, et al. Diffuse reflectance spectroscopy: diagnostic accuracy of a non-invasive screening technique for early detection of malignant changes in the oral cavity. BMJ Open 2011;1:e000071.
[19] Jayanthi JL, Subhash N, Stephen M, et al. Comparative evaluation of the diagnostic performance of autofluorescence and diffuse reflectance in oral cancer detection: a clinical study. J Biophotonics 2011;4:696–706.
[20] Kamath SD, Mahato KK. Optical pathology using oral tissue fluorescence spectra: classification by principal component analysis and *k*-means nearest neighbor analysis. J Biomed Opt 2007;12.
[21] Kan CW, Jiang BC, Nieman LT, et al. Comparison of linear and non-linear classifiers for oral cancer screening by optical spectroscopy. AMIA Ann Symp Proc/AMIA Symp AMIA Symp 2007: 1003.
[22] Majumder SK, Ghosh N, Gupta PK. Support vector machine for optical diagnosis of cancer. J Biomed Opt 2005;10.
[23] Majumder SK, Gupta A, Gupta S, et al. Multi-class classification algorithm for optical diagnosis of oral cancer. J Photochem Photobiol B 2006;85:109–17.
[24] Mallia R, Thomas SS, Mathews A, et al. Oxygenated hemoglobin diffuse reflectance ratio for in vivo detection of oral pre-cancer. J Biomed Opt 2008;13.
[25] Mallia RJ, Narayanan S, Madhavan J, et al. Diffuse reflection spectroscopy: an alternative to autofluorescence spectroscopy in tongue cancer detection. Appl Spectrosc 2010;64:409–18.
[26] Mallia RJ, Subhash N, Mathews A, et al. Clinical grading of oral mucosa by curve-fitting of corrected autofluorescence using diffuse reflectance spectra. Head Neck – J Sci Spec 2010;32:763–79.
[27] Manhas S, Swami MK, Patel HS, et al. Polarized diffuse reflectance measurements on cancerous and noncancerous tissues. J Biophotonics 2009;2:581–7.
[28] Mcgee S, Mardirossian V, Elackattu A, et al. Anatomy-based algorithms for detecting oral cancer using reflectance and fluorescence spectroscopy. Ann Otol Rhinol Laryn 2009;118:817–26.
[29] Schwarz RA, Gao W, Weber CR, et al. Noninvasive evaluation of oral lesions using depth-sensitive optical spectroscopy. Cancer 2009;115:1669–79.
[30] Sharwani A, Jerjes W, Salih V, et al. Assessment of oral premalignancy using elastic scattering spectroscopy. Oral Oncol 2006;42:343–9.
[31] Subhash N, Mallia JR, Thomas SS, et al. Oral cancer detection using diffuse reflectance spectral ratio R540/R575 of oxygenated hemoglobin bands. J Biomed Opt 2006;11.
[32] Vishwanath K, Yuan H, Barry WT, et al. Using optical spectroscopy to longitudinally monitor physiological changes within solid tumors. Neoplasia 2009;11:889–900.
[33] Palmer GM, Ramanujam N. Monte Carlo-based inverse model for calculating tissue optical properties. Part I: theory and validation on synthetic phantoms. Appl Opt 2006;45:1062–71.
[34] Vishwanath K, Chang K, Klein D, et al. Portable, fiber-based, diffuse reflection spectroscopy (DRS) systems for estimating tissue optical properties. Appl Spectrosc 2011;65:206–15.
[35] Hughes ORSN, Kraft M, Arens C, Birchall MA. Optical and molecular techniques to identify tumor margins within the larynx. Head Neck 2010; 32:1544–53.
[36] Perelman LT, Backman V, Wallace M, et al. Observation of periodic fine structure in reflectance from biological tissue: a new technique for measuring nuclear size distribution. Phys Rev Lett 1998;80:627–30.
[37] Nieman L, Myakov A, Aaron J, et al. Optical sectioning using a fiber probe with an angled illumination-collection geometry: evaluation in engineered tissue phantoms. Appl Opt 2004;43:1308–19.

[38] Ross MH, Pawlina W. Histology: a text and atlas: with correlated cell and molecular biology. 5th ed. Baltimore, MD: Lippincott Williams & Wilkins; 2006. p. xvii, 906 p.
[39] Koch WM. Head and neck cancer. In: Early diagnosis and treatment of cancer. Philadelphia, PA: Saunders/Elsevier; 2010. p. 1 online resource (xii, p. 255).
[40] Liu Q, Ramanujam N. Scaling method for fast Monte Carlo simulation of diffuse reflectance spectra from multilayered turbid media. J Opt Soc Am A 2007;24:1011–25.
[41] Bashkatov AN, Genina EA, Kochubey VI, et al. Optical properties of human skin, subcutaneous and mucous tissues in the wavelength range from 400 to 2000 nm. J Phys D Appl Phys 2005;38:2543–55.
[42] Upile T, Jerjes W, Betz CS, et al. Optical diagnostic techniques in the head and neck. Dent Update 2007;34:410–2. 15-6, 19-20 passim.
[43] Swinson B, Jerjes W, El-Maaytah M, et al. Optical techniques in diagnosis of head and neck malignancy. Oral Oncol 2006;42:221–8.
[44] Nordsmark M, Bentzen SM, Rudat V, et al. Prognostic value of tumor oxygenation in 397 head and neck tumors after primary radiation therapy. An international multi-center study. Radiother Oncol: J Eur Soc Ther Radiol Oncol 2005;77:18–24.
[45] Janssen HL, Haustermans KM, Balm AJ, et al. Hypoxia in head and neck cancer: how much, how important? Head Neck 2005;27:622–38.
[46] Terris DJ, Dunphy EP. Oxygen tension measurements of head and neck cancers. Arch Otolaryngol – Head Neck Surg 1994;120:283–7.
[47] Tryggvason K, Hoyhtya M, Salo T. Proteolytic degradation of extracellular-matrix in tumor invasion. Biochim Biophys Acta 1987;907:191–217.
[48] Nicolson GL. Cancer metastasis – organ colonization and the cell-surface properties of malignant-cells. Biochim Biophys Acta 1982;695:113–76.
[49] Matrisian LM, Bowden GT. Stromelysin/transin and tumor progression. Semin Cancer Biol 1990;1:107–15.
[50] Bejarano PA, Noelken ME, Suzuki K, et al. Degradation of basement membranes by human matrix metalloproteinase 3 (stromelysin). Biochem J 1988;256:413–9.
[51] Saidi IS, Jacques SL, Tittel FK. Mie and Rayleigh modeling of visible-light scattering in neonatal skin. Appl Opt 1995;34:7410–8.
[52] Georgakoudi I, Jacobson BC, Van Dam J, et al. Fluorescence, reflectance, and light-scattering spectroscopy for evaluating dysplasia in patients with Barrett's esophagus. Gastroenterology 2001;120:1620–9.
[53] Pierce MC, Schwarz RA, Bhattar VS, et al. Accuracy of in vivo multimodal optical imaging for detection of oral neoplasia. Cancer Prev Res (Phila) 2012;5:801–9.